PROCEEDINGS of the
24th International Congress on Acoustics

October 24 to 28, 2022 in Gyeongju, Korea

ABS-0788

Optimization Methods for Fixed Virtual Sensing Feedback ANC Controllers Targeting In-Ear Headphones

Piero RIVERA BENOIS[1,3]; Reinhild RODEN[2]; Matthias BLAU[2,3]; Simon DOCLO[1,3]

[1] Signal Processing Group, University of Oldenburg, Oldenburg, Germany

[2] Institut für Hörtechnik und Audiologie, Jade Hochschule, Oldenburg, Germany

[3] Cluster of Excellence Hearing4all, Germany

ABSTRACT

Active Noise Cancellation (ANC) applied to headphones aims at minimizing the environmental noise at the listener's ears. In this contribution, we consider an in-ear headphone equipped with an inner microphone and one loudspeaker and we compare different virtual sensing approaches (remote microphone technique, virtual microphone arrangement) to derive a fixed feedback ANC controller, minimizing the sound pressure at the ear drum instead of at the inner microphone. Based on multiple measurement sets of the acoustic paths between the loudspeaker, the noise source and the ear drum, we derive robust optimization methods to compute the FIR filter coefficients of the ANC controller, minimizing the power spectral density at the ear drum subject to design and stability constraints. Simulation results for diffuse noise and considering multiple reinsertions of the in-ear headphone show an improvement of the noise attenuation at the ear drum using the virtual sensing approaches, when compared to a classical approach optimized at the inner microphone.

Keywords: Virtual Sensing, Active Noise Cancellation, Headphones

1. INTRODUCTION

Active Noise Cancellation (ANC) applied to headphones aims at minimizing the environmental noise at the listener's ears. The working principle of ANC is based on the destructive superposition of sound waves, in this context the sound wave of the environmental noise reaching the listener's ear and the sound wave generated by the loudspeaker of the headphone (see the overview paper in [1]). In this paper we consider an in-ear headphone with an inner microphone and one loudspeaker and we aim at minimizing the sound pressure at the ear drum by means of a fixed feedback ANC controller. Since the sound pressure at the inner microphone and the ear drum are not equal [7], several virtual sensing techniques have been proposed (see the literature review in [5]) that exploit measurements performed during a calibration stage to move the zone of quiet from the position of the inner microphone to the position of the ear drum. In [2] a convex optimization method was proposed to derive the FIR filter coefficients of the ANC controller using the virtual microphone arrangement (VMA) approach, exploiting the proximity of the inner microphone to the ear drum to minimize the sound pressure at the ear drum. In [6],[7] non-convex optimization methods were proposed to derive the IIR filter coefficients of the ANC controller using the remote microphone technique (RMT) approach, relying only on the coherence between the sound pressure at the positions of the inner microphone and the ear drum to minimize the sound pressure at the ear drum.

In this work, we propose two convex optimization methods to derive the FIR filter coefficients of the ANC controller using the RMT and VMA approaches, which are robust against reinsertions of the headphones. Additionally, we show that the VMA approach [2] and the (non-virtual-sensing) minimum variance control (MVC) approach [3] are special cases of the proposed RMT approach.

This paper is structured as follows: Firstly, a description of the virtual sensing technique used in this work will be presented. Secondly, the proposed optimization methods for the design of the ANC controllers are described. Fourthly, simulations results based on acoustic transfer functions measured with an in-ear headphone prototype are presented to validate the proposed optimization methods.

[1] piero.rivera.benois@uni-oldenburg.de

2. FEEDBACK VIRTUAL SENSING

The virtual sensing algorithms that we consider use a two-stage approach (see Figure 1) . In the first stage, called calibration stage, a probe tube microphone (PTM) is placed at the ear drum. Afterwards, the in-ear headphone is inserted into the ear canal and the acoustic path between the loudspeaker and the ear drum, called the secondary path $S(z)$, is measured. Subsequently, a calibration noise field is generated around the user to measure the transfer function $\widehat{M}(z) = \widehat{\Phi}_{dr}(z)/\widehat{\Phi}_{rr}(z)$ between the inner microphone and ear drum, where $\widehat{\Phi}_{dr}(z)$ and $\widehat{\Phi}_{rr}(z)$ denote the cross- and auto-correlation functions in the z-transform domain estimated from the signals measured at the inner microphone and the PTM (ear drum). After removing the PTM, the in-ear headphone is reinserted and the acoustic path between the loudspeaker and the inner microphone, called the feedback path $B_r(z)$, is measured.

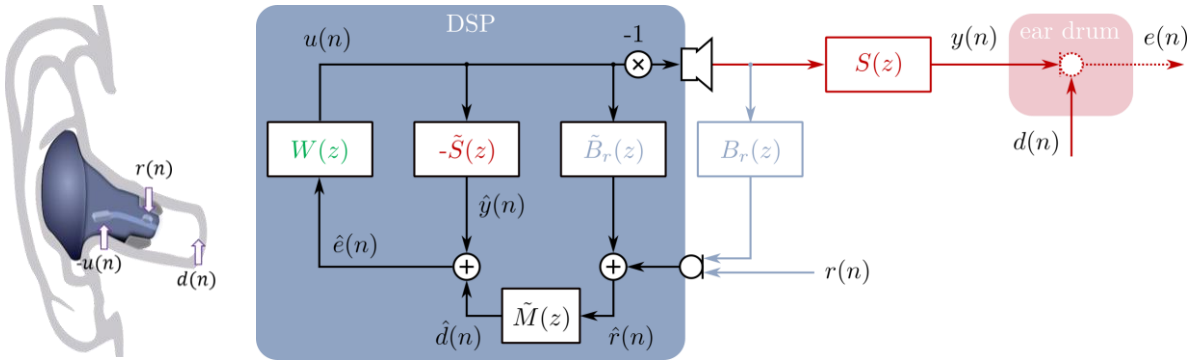

Figure 1. On the left, an in-ear headphone with an inner microphone and one loudspeaker, $r(n)$ and $d(n)$ denote the signals generated by the incident noise arriving at the inner microphone and the ear drum, respectively, and $u(n)$ denotes the loudspeaker signal generated by the ANC controller. On the right, the block diagram of the proposed ANC controller implementing a virtual sensing algorithm.

During the second stage, called control stage, it is assumed that the measured acoustic paths to the ear drum remain more or less unchanged after removing the PTM and reinserting the in-ear headphone. The measured acoustic paths $\hat{S}(z)$, $\widehat{M}(z)$ and $\hat{B}_r(z)$ are used as internal models $\tilde{S}(z)$, $\tilde{M}(z)$ and $\tilde{B}_r(z)$ by in the virtual sensing algorithm in Figure 1 to make an on-line estimation of the sound pressure at the ear drum $e(n)$. The estimated sound pressure at the ear drum $\hat{e}(n)$ is used as input for the controller $W(z)$.

The power spectral density (PSD) of $e(n)$ at frequency f can be written as follows

$$\Phi_{ee}(f) = \left(1 - \frac{|\Phi_{dr}(f)|^2}{\Phi_{dd}(f)\Phi_{rr}(f)}\right)\Phi_{dd}(f) + \left|\frac{\Phi_{dr}(f)}{\Phi_{rr}(f)} - \frac{\tilde{M}(f)W(f)S(f)}{1 + W(f)\left(\tilde{S}(f) + \tilde{M}(f)\left(B_r(f) - \tilde{B}_r(f)\right)\right)}\right|^2 \Phi_{rr}(f).$$

The left-hand term determines the minimum achievable PSD $\Phi_{ee}(f)$, which is only equal to zero when the magnitude squared coherence between $r(n)$ and $d(n)$ is equal to 1. The right-hand term defines the scope of the optimization, where it should be noted that both numerator as well as denominator depend on the controller $W(f)$.

For the virtual sensing approaches (RMT and VMA) it is assumed that the secondary path $S(z)$ remains unchanged after removing the PTM and reinserting the in-ear headphone. In addition it is assumed that the changes in the feedback path $B_r(z)$ can be compensated with state-of-the-art on-line estimations methods. When using the RMT approach, it is assumed that for the external noise source the sound pressure at the inner microphone and the ear drum are related by $d(n) = m(n) * r(n)$, and consequently, $\frac{\Phi_{dr}}{\Phi_{rr}} = M(f)$, such that if these assumptions are applied to the previous equation, the PSD at the ear drum Φ_{ee} simplifies to

$$\Phi_{ee}^{\mathrm{RMT}}(f) = \left|M(f) - \tilde{M}(f)\frac{W(f)\tilde{S}(f)}{1 + W(f)\tilde{S}(f)}\right|^2 \Phi_{rr}(f).$$

Alternatively, when using the VMA approach, it is assumed that for the external noise source the

sound pressure at the inner microphone and at the ear drum are equal, i.e. $d(n) = r(n)$. Hence, the internal model $\widetilde{M}(z)$ in Figure 1 is set to $\widetilde{M}(z) = 1$ and the PSD at the ear drum reduces to

$$\Phi_{ee}^{\mathrm{VMA}}(f) = \left|\frac{1}{1 + W(f)\tilde{S}(f)}\right|^2 \Phi_{rr}(f).$$

In contrast to the virtual sensing approaches, when using the (non-virtual-sensing) MVC approach, it is assumed that the secondary and feedback paths are equal, i.e. $S(z) = B_r(z)$ and, therefore, the internal models $-\tilde{S}(z)$ and $\tilde{B}_r(z)$ in Figure 1 are removed and the PSD at the ear drum reduces to

$$\Phi_{ee}^{\mathrm{MVC}}(f) = \left|\frac{1}{1 + W(f)\tilde{B}_r(f)}\right|^2 \Phi_{rr}(f),$$

which is equal to the PSD at the inner microphone. As can be observed from the last three equations, the optimization of the controller $W(z)$ by minimization of the objective functions $\Phi_{ee}^{\mathrm{RMT}}(f)$, $\Phi_{ee}^{\mathrm{VMA}}(f)$ and $\Phi_{ee}^{\mathrm{MVC}}(f)$ is a non-convex optimization problem, because the denominators depend on the controller $W(f)$. Instead of directly minimizing the objective functions, we propose to derive the controller $W(z)$ by satisfying the optimality conditions resulting in the minimum achievable PSD at the ear drum. For the RMT approach, the optimality condition $\left|W(f)\tilde{S}(f)\right| \gg 1$ results in the minimum achievable PSD

$$\Phi_{ee}^{\mathrm{RMT,opt}}(f) = \left|M(f) - \widetilde{M}(f)\right|^2 \Phi_{rr},$$

which depends on the similarity between the internal model $\widetilde{M}(f)$ and the real system $M(f)$. For the VMA approach, the optimality condition $\left|1 + W(f)\tilde{S}(f)\right| \gg 1$ results in the minimum achievable PSD

$$\Phi_{ee}^{\mathrm{VMA,opt}}(f) = 0.$$

Similarly, for the MVC approach the optimality condition $\left|1 + W(f)\tilde{B}(f)\right| \gg 1$ results in the minimum achievable PSD

$$\Phi_{ee}^{\mathrm{MVC,opt}}(f) = 0.$$

3. CONTROLLER DESIGN

Instead of deriving the controller $W(z)$ by minimizing the non-convex objective functions Φ_{ee}^{RMT}, Φ_{ee}^{VMA} and Φ_{ee}^{MVC}, we propose to satisfy the optimality conditions presented in the previous section as well as possible, resulting in convex optimization problems in the discrete Fourier transform (DFT) domain. We assume $W(z)$ to be an FIR filter with N filter coefficients stacked in the vector $\boldsymbol{w}$. For the RMT controller, the optimality conditions to be satisfied is $\left|W(f)\tilde{S}(f)\right| \gg 1$, resulting in the convex maximization problem in the DFT domain

$$\boldsymbol{w}_{\mathrm{RMT}} = \arg\max_{\boldsymbol{w}} \sum_{k=0}^{\frac{L_{DFT}}{2}-1} \left|W(\Omega_k)\tilde{S}(\Omega_k)\right|^2 \left|\widetilde{M}(\Omega_k)\right|^2 G_1^2(\Omega_k),$$

where $\tilde{S}(\Omega_k)$ is the frequency responses of the secondary path internal model $\tilde{S}(z)$, k denotes the frequency index, L_{DFT} denotes the DFT length, $G_1(\Omega_k)$ denotes a frequency dependent function to weight the low frequencies more than the mid and high frequencies and the squared magnitude response of the internal model $\left|\widetilde{M}(\Omega_k)\right|^2$ is used to weight lower the frequencies that are attenuated by $M(z)$. For the VMA and MVC controllers, the optimality condition to be satisfied is $\left|1 + W(f)\tilde{S}(f)\right| \gg 1$ and $\left|1 + W(f)\tilde{B}_r(f)\right| \gg 1$, respectively. Hence, as in [2] and [3] the corresponding convex maximization problems can be formulated as

$$\boldsymbol{w}_{\mathrm{VMA}} = \arg\max_{\boldsymbol{w}} \sum_{k=0}^{\frac{L_{DFT}}{2}-1} \left|1 + W(\Omega_k)\tilde{S}(\Omega_k)\right|^2 G_1^2(\Omega_k)$$

and

$$\boldsymbol{w}_{\mathrm{MVC}} = \arg\max_{\boldsymbol{w}} \sum_{k=0}^{\frac{L_{DFT}}{2}-1} \left|1 + W(\Omega_k)\tilde{B}_r(\Omega_k)\right|^2 G_1^2(\Omega_k).$$

It should be noted that the VMA and MVC approaches do not require the frequency response $\widetilde{M}(\Omega_k)$, and, therefore, their calibration stage does not require a calibration noise field. Moreover, the MVC approach only requires $\tilde{B}_r(\Omega_k)$, hence, no PTM is needed for its calibration stage.

Aiming at deriving a controller $W(z)$ that yields a stable system, a stability constraint is imposed. Similarly as in [2], the solution space is restricted by a single-sided hyperbolic boundary. However, aiming at producing a quadratic dependency w.r.t. $W(\Omega_k)$, we propose to formulate the stability

constraint as an inequality between quadratic terms as

$$\left|\varrho - W(\Omega_k)\tilde{S}(\Omega_k)\right|^2 \leq \left(\left|\varrho + W(\Omega_k)\tilde{S}(\Omega_k)\right| + 2\cdot\rho\right)^2,$$

where ϱ determines the focus $(-\varrho, 0)$ and ρ the x-axis intersect $(-\rho, 0)$ of the hyperbola. In addition, in order to limit the maximum gain of the controller $W(z)$, the convex inequality constraint

$$|W(\Omega_k)|^2 \leq G_3^2(\Omega_k)$$

is introduced, where $G_3(\Omega_k)$ denotes the maximum allowed gain. Feedback ANC approaches are generally subject to the water-bed effect and therefore prone to produce amplifications outside the attenuation bandwidth [7]. Aiming at restricting such amplification, we propose to introduce the following convex inequality constraint

$$\left|1 + W(\Omega_k)\tilde{S}(\Omega_k)\left(1 - {\tilde{M}(\Omega_k)}/{\hat{M}(\Omega_k)}\right)\right|^2 \leq G_2^2(\Omega_k)\left|1 + W(\Omega_k)\tilde{S}(\Omega_k)\right|^2$$

for the optimization of the RMT controller, where $G_2(\Omega_k)$ denotes the maximum allowed amplification and differences between $\tilde{M}(\Omega_k)$ and $\hat{M}(\Omega_k)$ are considered. Since for the VMA controller the frequency responses $\tilde{M}(\Omega_k)$ and $\hat{M}(\Omega_k)$ are set to 1, the previous inequality constraint reduces to

$$1 \leq G_2^2(\Omega_k)\left|1 + W(\Omega_k)\tilde{S}(\Omega_k)\right|^2.$$

Similarly, for the optimization of the MVC controller, $\tilde{S}(\Omega_k)$ is replaced by $\tilde{B}_r(\Omega_k)$ in this constraint, i.e.

$$1 \leq G_2^2(\Omega_k)\left|1 + W(\Omega_k)\tilde{B}_r(\Omega_k)\right|^2.$$

The proposed convex maximization problems subject to the aforementioned constraints can then be solved using SQP algorithms, e.g., implemented in the MATLAB function `fmincon()`. During all optimizations in this work we used $N = 128$ filter coefficients, $L_{DFT} = 8192$, $\varrho = 0.8$ and $\rho = 0.9$. Similarly to [2], we used the frequency-dependent functions $G_1(f)$, $G_2(f)$and $G_3(f)$ depicted in Figure 2.

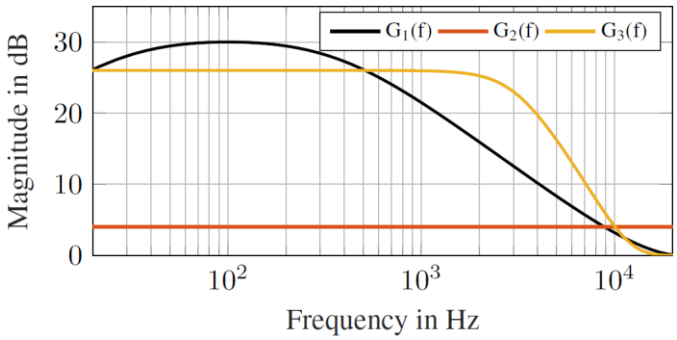

Figure 2. Frequency-dependent functions: $G_1(f)$ is the frequency-weighting function used in the objective function, $G_2(f)$ is the maximum allowed amplification of 4 dB due to water-bed effect and $G_3(f)$ is the maximum controller gain of 26 dB in the low frequencies.

4. SIMULATIONS

In this section, the performance of the proposed RMT and VMA controllers is compared to the performance of the MVC controller for a diffuse noise field using the inner microphone and one loudspeaker of the in-ear headphone prototype described in [4]. The acoustic transfer functions between the loudspeakers and the inner microphone $B_r(z)$ and the ear drum $S(z)$ were measured in [4] for several reinsertions of the in-ear headphone prototype in the ear of a subject using a probe tube microphone. All simulations were performed at a sampling frequency of $f_s = 44.1$ kHz. From the database in [4] eight measurement sets were considered. Using one measurement set, the measured secondary path $\hat{S}(z)$ was used and a diffuse calibration noise field was generated to determine the transfer function $\hat{M}(z) = \hat{\Phi}_{dr}(z)/\hat{\Phi}_{rr}(z)$. The RMT controller was optimized considering using the transfer functions $\hat{S}(z)$ and $\hat{M}(z)$, whereas the VMA controller was optimized using only the transfer function $\hat{S}(z)$. Using the remaining seven measurement sets, seven reinsertions of the in-ear headphone were simulated. After each reinsertion, the MVC controller was re-optimized considering a perfect measurement of the respective feedback path, i.e. $\hat{B}_r(z) = B_r(z)$. For each reinsertion a control stage of the RMT, VMA and MVC controllers was simulated. For the RMT control stage all

three internal models $\tilde{B}_r(z)$, $\tilde{M}(z)$ and $\tilde{S}(z)$ in Figure 1 are required. For the VMA control stage only $\tilde{B}_r(z)$ and $\tilde{S}(z)$ are required, because $\tilde{M}(z)$ is set to one. For the MVC control stage no internal model is required. For the RMT and VMA control stages, the internal model of the feedback path was assumed to be perfect, i.e. $\tilde{B}_r(z) = B_r(z)$. The internal model of the secondary path was set to the secondary path measured during the calibration stage, i.e. $\tilde{S}(z) = \hat{S}(z)$. The internal model $\tilde{M}(z)$ was derived using a causal FIR approximation [8] of the transfer function $\hat{M}(z)$ determined during the calibration stage.

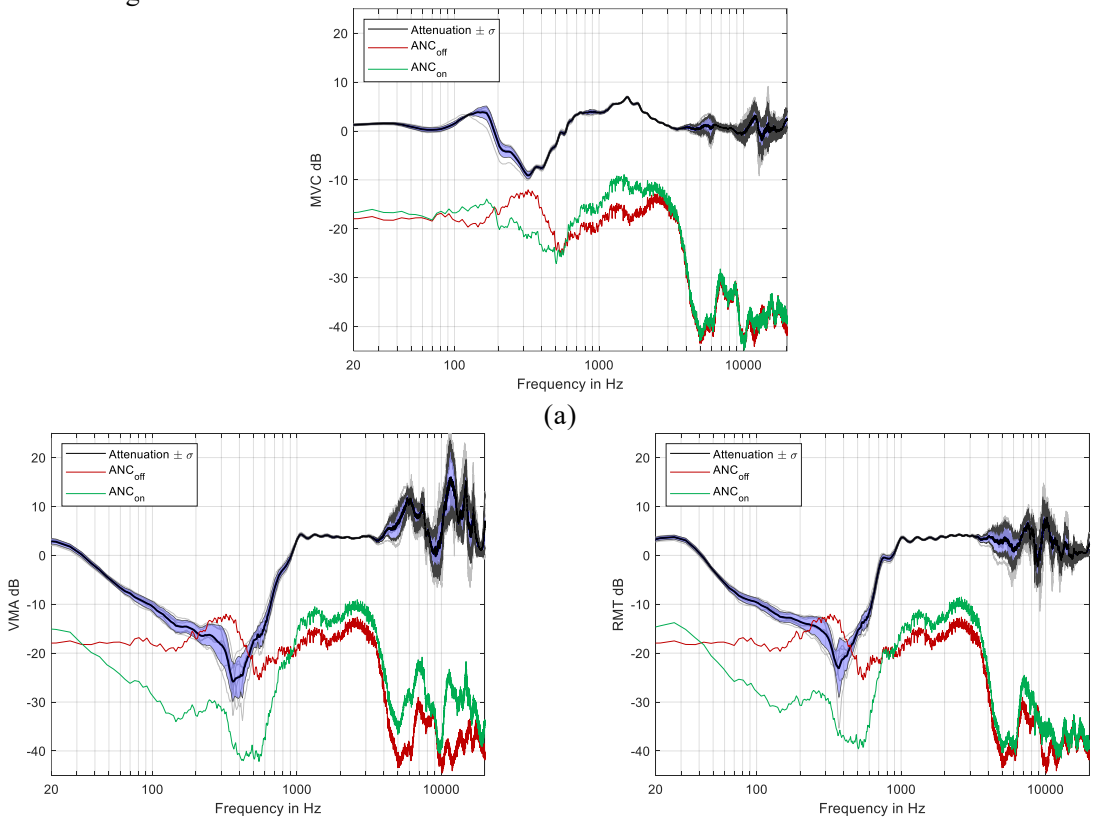

Figure 3. Simulation results for (a) the MVC controller, (b) the VMA controller and (c) the RMT controller. $\mathrm{ANC_{off}}$ and $\mathrm{ANC_{on}}$ correspond to PSDs at the ear drum when ANC is turned off and on, respectively. $\mathrm{Attenuation} \pm \sigma$ corresponds to the mean attenuation curve alongside the standard deviation calculated using seven reinsertions of the in-ear headphone in [4].

Figure 3 depicts the PSDs of the sound pressure at the ear drum $\Phi_{ee}(f)$ with ANC off and ANC on, using either the MVC, the VMA or the RMT controller. In the same plot the mean attenuation curve is presented alongside the standard deviation calculated using the seven reinsertions. Please note that when the mean attenuation is smaller than 0 dB attenuation is produced and, otherwise, amplification is produced instead. In addition, it should be noted that none of the re-insertions produced an unstable system, which corroborates that the proposed optimization method yields a robust controller. First, it can be observed from ANC off that the passive attenuation of the in-ear headphone is very high for frequencies above 4 kHz. Second, it can be observed in Figure 3 (a) that the attenuation achieved by the MVC controller is limited to the bandwidth between 200 to 550 Hz with a maximum magnitude of approx. 10 dB. In the frequency regions before and after the attenuation bandwidth a water-bed effect is visible, which exceeds the limit of 4 dB imposed by $G_2(f)$ at about 1.5 kHz. This may be due to the fact that the assumptions of the MVC approach do not hold for frequencies above 1 kHz. Third, it can be observed in Figure 3 (b) that the attenuation achieved by the VMA controller is much higher both in terms of bandwidth and magnitude when compared to the MVC controller. Furthermore, although the water-bed effect is controlled for frequencies below 4 kHz, amplifications of up to 25 dB can be observed at higher frequencies. This may be due to the fact that the assumption of the MVA controller, i.e. $d(n) = r(n)$, does not hold in this frequency region,

because the wave lengths are comparable to the distance between the inner microphone and the ear drum. Finally, it can be observed in Figure 3 (c) that the attenuation achieved by the RMT controller is slightly inferior when compared to the attenuation achieved by the VMA controller. However, the water-bed effect produced in the high frequencies is much lower when compared to the water-bed effect produced by the VMA controller. The fact that the water-bed effect is still higher than 4 dB may be due to the variability of the system $M(z)$ in the high frequencies.

5. CONCLUSIONS

In this paper, we considered an in-ear headphone equipped with an inner microphone and one loudspeaker and proposed two optimization methods based on the RMT and VMA approaches to derive a fixed feedback ANC controller, minimizing the sound pressure at the ear drum instead of at the inner microphone. The optimization methods require a calibration stage during which a PTM is inserted into the ear and the acoustic paths between the loudspeaker, the noise source and the ear drum are measured. We proposed to use optimality conditions to formulate convex objective functions resulting in the minimum achievable PSD at the ear drum, subject to convex stability and design constraints. Furthermore, aiming at a better control of the water-bed effect in the high frequencies, a new constraint was proposed for the optimization of the RTM controller. The new constraint exploits the acoustic path measured between the inner microphone and the ear drum with an external calibration noise field. Simulation results for diffuse noise and considering multiple reinsertions of the in-ear headphone corroborated that the ANC controllers derived with the proposed optimization methods are robust against reinsertions of the device. A considerable improvement of the noise attenuation at the ear drum could be observed when comparing the RMT and VMA approaches to the classical MVC approach optimized at the inner microphone. While the RMT controller achieves a better control of the amplification outside of the attenuation bandwidth when compared to the VMA controller, the VMA controller achieves the highest attenuation bandwidth and magnitude among the evaluated controllers. In future work the optimization methods will be extended for in-ear headphones with multiple loudspeakers, and by integrating uncertainty models of the acoustic transfer functions, e.g., produced by intra-subject variability.

ACKNOWLEDGEMENTSs

This work was funded by the Deutsche Forschungsgemeinschaft (DFG, German Research Foundation) under Germany's Excellence Strategy - EXC 2177/1 - Project ID 390895286 and Project ID 352015383 - SFB 1330 C1.

REFERENCES

1. Kajikawa, Y., Gan, W., & Kuo, S. (2012). Recent advances on active noise control: Open issues and innovative applications. APSIPA Transactions on Signal and Information Processing, 1, E3. doi:10.1017/ATSIP.2012.4.
2. P. Rivera Benois, R. Roden, M. Blau, and S. Doclo. Optimization of a fixed virtual sensing feedback anc controller for in-ear headphones with multiple loudspeakers. In Proc. IEEE International Conference on Acoustics, Speech and Signal Processing (ICASSP), pages 8717–8721., 2022.
3. P. Rivera Benois. Hybrid and Pseudo-Cascaded Active Noise Control Applied to Headphones. PhD thesis, Helmut-Schmidt-Universität / Universität der Bundeswehr Hamburg, Hamburg, December 2020.
4. F. Denk and B. Kollmeier. The hearpiece database of individual transfer functions of an in-the-ear earpiece for hearing device research. Acta Acust., 5:2, 2021.
5. D. Moreau, B. Cazzolato, A. Zander, and C. Petersen, A review of virtual sensing algorithms for active noise control, Algorithms, vol. 1, p. 69–99, Nov 2008.
6. Z. Zhang, M. Wu, L. Yin, C. Gong, J. Wang, S. Zhou, J. Yang, Robust feedback controller combined with the remote microphone method for broadband active noise control in headrest, Applied Acoustics, Volume 195, 2022.
7. F. An, Q. Wu, and B. Liu, Feedback controller optimization for active noise control headphones considering frequency response mismatch between microphone and human ear, Applied Sciences, vol. 12, no. 3, 2022.
8. P. Rivera Benois, P. Bhattacharya, and U. Zölzer, Derivation technique for headphone transfer functions based on sine sweeps and least squares minimization, In Proc. INTER-NOISE and NOISE-CON Congress and Conference, vol. 253, no. 4, 2016.